O_2 and N_2O Activation by Bi-, Tri-, and Tetranuclear Cu Clusters in Biology

EDWARD I. SOLOMON,* RITIMUKTA SARANGI, JULIA S. WOERTINK, ANTHONY J. AUGUSTINE, JUNGJOO YOON, AND SOMDATTA GHOSH

Department of Chemistry, Stanford University, Stanford, California 94305

Received December 21, 2006

ABSTRACT

Copper-cluster sites in biology exhibit unique spectroscopic features reflecting exchange coupling between oxidized Cu's and e^- delocalization in mixed valent sites. These novel electronic structures play critical roles in O_2 binding and activation for electrophilic aromatic attack and H-atom abstraction, the $4e^-/4H^+$ reduction of O_2 to H_2O, and in the $2e^-/2H^+$ reduction of N_2O. These electronic structure/reactivity correlations are summarized below.

1. Introduction

Cu proteins play central roles in Fe, Cu, and O_2 metabolism, are related to a range of genetic diseases, and are important in biotechnology, detoxification, and the elimination of greenhouse gases. Understanding Cu biochemistry on a molecular level provides mechanisms to improve or inhibit these processes and enhance drug design. The Cu proteins involved in O_2 binding, activation, and reduction to H_2O and the reduction of N_2O to water and dinitrogen are summarized in Figure 1. The term "coupled" is used here to refer to the antiferromagnetic (AF) "coupling" between paramagnetic metal centers that can lead to a diamagnetic $S_{tot} = 0$ ground state. If two Cu^{II}'s, $S = {}^1/_2$, directly overlap, they will spin pair. If, however, they are far enough apart so that their d orbitals do not directly overlap but have a bridging ligand, this can provide a superexchange pathway (i.e., a delocalized molecular orbital) between the two paramagnetic Cu^{II}'s that results in their spin pairing, indirectly through overlap with the bridge. This is described by the exchange Hamiltonian $H = -2JS_AS_B$, which spin couples the two $S = {}^1/_2$'s on Cu_A and Cu_B to form total spins $S_{tot} = 1$ and 0, where for AF coupling the $S_{tot} = 0$ is lower in energy by $2J$ ($J < 0$).

In this paper, we will (1) consider the unique spectral features of the coupled binuclear Cu proteins, hemocyanin (Hc), catechol oxidase, and tyrosinase (Ty), that reflect a novel electronic structure that allows their reversible binding of O_2 (a spin-forbidden process) and its activation for electrophilic attack on an aromatic substrate by Ty, (2) contrast this electronic structure to that of the noncoupled binuclear Cu enzymes (i.e., no magnetic interaction between the two Cu^{II}'s $S = {}^1/_2$) to evaluate the contribution of these differences in AF exchange coupling to the reaction mechanisms, where the noncoupled binuclear Cu sites in dopamine β-monooxygenase (DβM) and peptidylglycine α-hydroxylating monooxygenase (PHM) activate O_2 for H-atom abstraction, (3) extend these studies to the trinuclear Cu cluster site in the multicopper oxidases, where the exchange coupling among the three coppers plays a central role in the $4e^-/4H^+$ reduction of O_2 to H_2O, and (4) consider how the interactions among the coppers in the μ_4-sulfide bridged tetranuclear Cu_z cluster promote the $2e^-/2H^+$ cleavage of the N–O bond by N_2O reductase.

2. Coupled Binuclear Copper Proteins

From spectroscopy and crystallography, Hc (reversible O_2 binding), catechol oxidase (O_2 binding and catechol oxidation to quinone), and Ty (O_2 binding, oxidation, and monooxygenation of phenol to catechol) all have equivalent geometries (μ-η^2:η^2 $Cu^{II}_2O_2$, side-on peroxide-bridged binuclear Cu^{II} sites coordinated to the protein by three His ligands on each Cu) and electronic structures (*vide infra*).[1] Their range of functions increases from Hc to Ty, which has been attributed to differences in substrate accessibility to their coupled binuclear Cu sites.

2.1. Unique Spectroscopic Features → Novel Electronic Structure. To understand the unique spectral features of the oxygenated sites of these proteins, we first consider what is normal for a Cu^{II}–peroxide bond. Cu^{II} is d^9 and thus has one half-occupied valence d orbital, either $d_{x^2-y^2}$ for tetragonal or d_{z^2} for trigonal bipyramidal geometries. Peroxide has a doubly degenerate highest occupied molecular orbital (HOMO) set, which will split in energy upon binding to Cu^{II}, with the π^*_σ being stabilized to a deeper binding energy because of σ bonding to the half-occupied d orbital and the π^*_v (vertical) not being very affected by bonding because it is perpendicular to the Cu^{II}–(O_2^{2-}) plane (Figure 2A).[2]

In a peroxide-bridged binuclear Cu^{II} complex as in the $[(TMPA)Cu]_2O_2$ dimer (trigonal bipyramidal at each Cu^{II}), one further has to take symmetric and antisymmetric combinations of the half-occupied d_{z^2} orbitals on the Cu's and then allow for bonding with the occupied peroxide π^* valence orbitals.[3] As shown in Figure 2B, only one combination of d_{z^2} orbitals has net σ overlap with the peroxide π^*_σ orbital causing stabilization of the π^*_σ orbital and a destabilization of the $d_{z^2A} + d_{z^2B}$ molecular orbital. This leads to spin pairing of the two electrons in the d_{z^2} orbitals of the two coppers and the antiferromagnetically coupled $S = 0$, singlet ground state. This also produces a peroxide $\pi^*_\sigma \rightarrow$ Cu ($d_{z^2A} + d_{z^2B}$) charge transfer (CT) transition as shown in Figure 3A. Resonance Raman (rR) excitation into this CT transition produces an O–O stretching vibration at ~830 cm^{-1} (Figure 3B), which is characteristic of peroxide bridging in a "normal" binuclear Cu^{II} complex.[3]

Ritimukta Sarangi, Julia Woertink, Anthony Augustine, Jungjoo Yoon, and Somdatta Ghosh are all graduate students in the lab of Edward Solomon, who is the Monroe E. Spaht Professor of Chemistry at Stanford University.

* To whom correspondence should be addressed. Fax: 650-725-0259. E-mail: Edward.Solomon@stanford.edu.

10.1021/ar600060t CCC: $37.00
Published on Web 05/02/2007

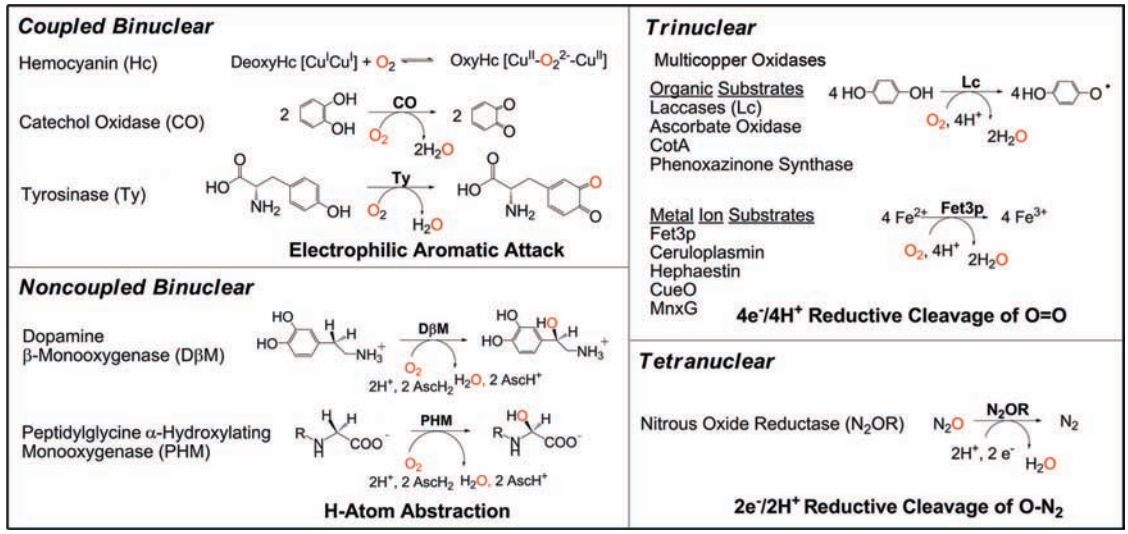

FIGURE 1. Multinuclear Cu sites in biology.

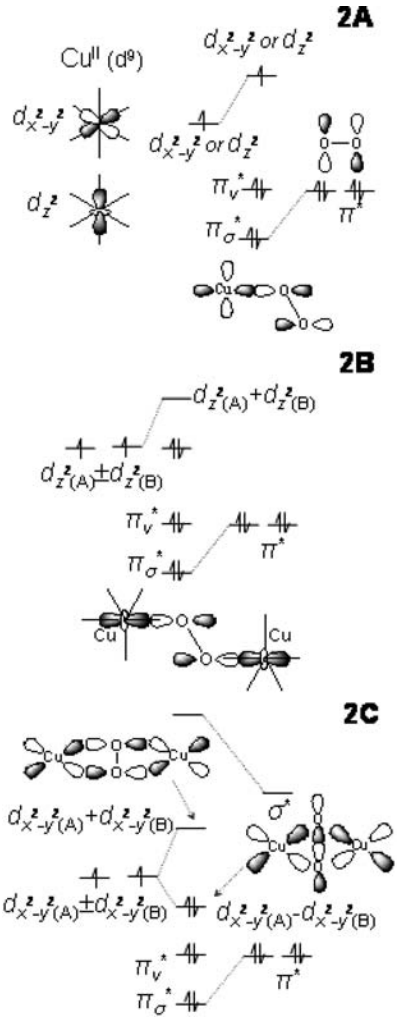

FIGURE 2. Electronic structure of the (A) end-on $Cu–O_2^{2-}$ complex, (B) end-on bridged $[Cu_2–O_2^{2-}]$ complex, and (C) side-on bridged OxyHc.

We now consider the unique geometric and electronic structure of oxy-Hc/oxy-Ty. Again, we take the symmetric and antisymmetric combination of the $d_{x^2-y^2}$ half-occupied valence orbitals of the two coppers (here, the ligand field of each Cu is square-pyramidal) and allow for their bonding interactions with the peroxide π^* valence orbitals but in the side-on peroxide-bridged structure of the oxy-Hc site (Figure 2C). Again, the π^*_σ orbital is stabilized, and the Cu $d_{x^2-y^2A} + d_{x^2-y^2B}$ is destabilized because of σ bonding. However, in the side-on bridged structure, there are two σ-bonding interactions of the peroxide with each copper and this leads to a very large bonding–antibonding interaction.[4] Thus, a strongly AF-stabilized singlet ground state and an intense O_2^{2-} $\pi^*_\sigma \rightarrow$ Cu $(d_{x^2-y^2A} + d_{x^2-y^2B})$ CT transition, which is shifted to a higher energy, are observed (green line versus black line in Figure 3A). Importantly, rR excitation into this CT transition shows a very low O–O stretching frequency (ν_{O-O}) at ~750 cm^{-1} (Figure 3B). The large peroxide σ donation of electron density from the π^*_σ orbital (which is antibonding with respect to the O–O bond) to the Cu^{II}'s should increase and not decrease the strength of the O–O bond. However, there is an additional bonding interaction that occurs in the side-on peroxide-bridged structure. The lowest unoccupied molecular orbital (LUMO) on the peroxide is the σ^* (Figure 2C), which bonds with the occupied $d_{x^2-y^2A} - d_{x^2-y^2B}$ combination of d orbitals on the Cu's, which is the HOMO. This back bonding shifts some of the electron density into the O_2^{2-} σ^* orbital, which is strongly antibonding with respect to the O–O bond and leads to the very low ν_{O-O}.[4]

In summary, the extremely covalent σ bonding between the two Cu^{II}'s through the μ-η^2:η^2 peroxide π^*_σ orbital leads to the AF-coupled singlet ground state, and the back bonding of the electron density from the Cu $(d_{x^2-y^2A} - d_{x^2-y^2B})$ HOMO into the peroxide σ^* LUMO leads to an extremely weak O–O bond activated for cleavage.

2.2. Reaction Coordinate for O_2 Binding. Deoxy-Hc/Ty with two d^{10} Cu^I centers binds triplet O_2 reversibly to form oxy-Hc/oxy-Ty, which has the AF-coupled singlet ground state. Thus, this reaction is spin-forbidden. To obtain a reaction coordinate for reversible O_2 binding, we started with the μ-η^2:η^2 structure, moved the peroxide out of the molecular plane, and geometry-optimized the rest

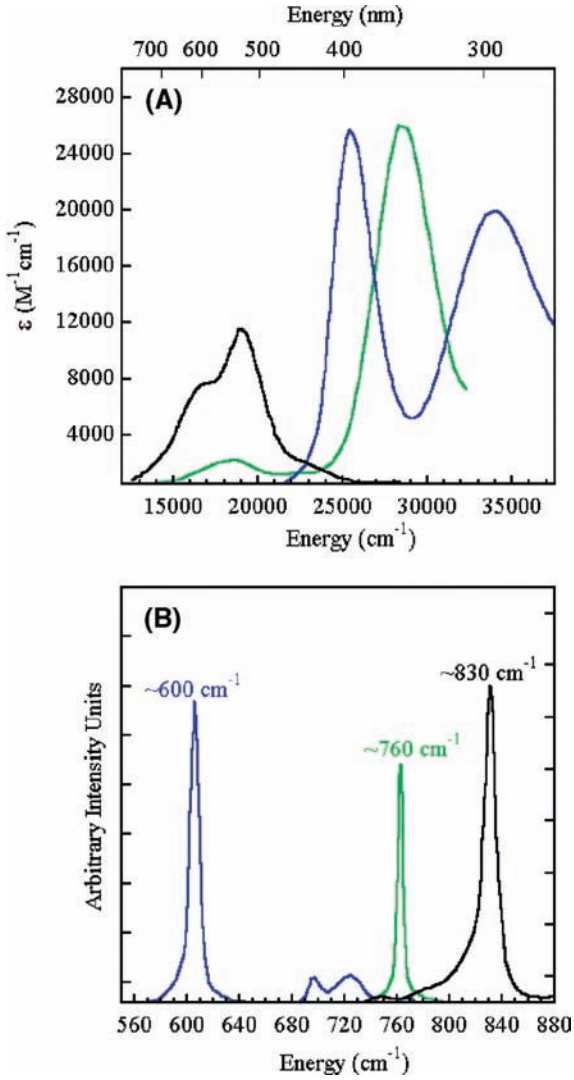

FIGURE 3. (A) Absorption and (B) resonance Raman spectra of $\{[(TMPA)Cu]_2O_2\}^{2+}$ (end-on; black line), $Cu[HB(3,5\text{-}i\text{-}Pr_2pz)_3]_2(O_2)$ (side-on; green line), and $\{[L^{TMCHD}Cu]_2O_2\}$ (bis-μ-oxo; blue line).

of the structure.[5] The structure first butterflies, then goes to a μ-η^1:η^2 asymmetric structure, and then to an end-on bridged structure in the reversible loss of O_2 (Figure 4A). These structures maximize the metal–ligand overlaps along this reaction coordinate. As the peroxide moves away from the coppers, its negative charge decreases as does the positive charge on the coppers. Thus, electron density is being transferred from the peroxide to the Cu^{II}'s. Importantly, both coppers are reduced at the same rate even in the asymmetric μ-η^1:η^2 structure. Thus, the reversible loss of peroxide as O_2 involves simultaneous two electron transfer.

In Figure 4B, we consider how the spin changes along this reaction coordinate. On the far left is the AF stabilization of the singlet ground state of the side-on peroxide-bridged structure through its π_o^* orbital. However, as the peroxide moves out of the molecular plane to the butterflied structure, the singlet/triplet splitting collapses and the triplet is in fact slightly lower in energy. This is because the spin on each Cu covalently delocalizes into a different peroxide π^* orbital. These are close to orthogonal in the butterflied structure, which favors the triplet ground state. From here, one electron of the same spin can be transferred from each π^* orbital to each Cu, leading to a loss of O_2 in its triplet $^3\Sigma_g^-$ ground state.[5]

Thus, the stabilization of the triplet ground state of O_2 is lost by charge transfer from the remote Cu's, and the singlet structure is then stabilized by the formation of an efficient superexchange pathway (the π_o^* orbital overlap) along the reaction coordinate.

2.3. Reaction Coordinate of Monooxygenation. In early literature, we found that oxy-Ty had the same geometric and electronic structure as oxy-Hc but that it differed from Hc in having substrate access and coordination directly to the copper in a trigonal-bipyramidal-distorted structure. This led to the generally accepted monooxygenation mechanism for oxy-Ty shown in Figure 5.[1,6,7] Phenolate substrate binds directly to the side-on peroxy-bridged oxy-Ty site (oxy-T). The trigonal pyramidal distortion leads to electrophilic attack and hydroxylation at the ortho position to produce a bound catecholate (met-D). Two-electron oxidation leads to the corresponding quinone product and a reduced (deoxy) site capable of O_2 binding for further turnover. The interesting issue now is whether the side-on oxy-Ty structure directly reacts with the aromatic ring or whether phenolate coordination leads to a bis-μ-oxo structure (*vide infra*) and performs the electrophilic attack on the ring.

The latter possibility was raised by the results of Tolman et al., who showed that the side-on peroxy-bridged structure could convert to the bis-μ-oxo structure with certain chelating ligands (Figure 6A).[8] Cu K pre-edge X-ray absorption data showed that conversion of the side-on to the bis-μ-oxo isomer leads to an increase in energy of the Cu 1s → 3d transition by 1.9 eV, indicating that the Cu^{II} is oxidized to Cu^{III} in the bis-μ-oxo structure.[9] The orbital correlation diagram for this interconversion is given in Figure 6B. Starting from the side-on bridged structure on the left, the O–O bond elongates from 1.4 to 2.3 Å in the bis-μ-oxo structure (the Cu–O distance goes from 1.92 to 1.81 Å). The O_2^{2-} σ^* orbital thus drops in energy to below the HOMO on the coppers, resulting in the oxidation to two Cu^{III}'s and reduction of the peroxide to the bridged oxide level.[10] This produces a low-energy, intense μ-O^{2-} → Cu ($d_{x^2-y^2A} - d_{x^2-y^2B}$) LUMO CT transition (blue line in Figure 3A), and rR excitation into this transition now shows an intense vibrational peak at 600 cm^{-1}, corresponding to the $Cu_2(O)_2$ symmetric stretch (Figure 3B). Thus, we now have two LUMOs that are frontier molecular orbitals (FMOs) capable of electrophilic attack on the occupied π orbitals of the aromatic ring (Figure 6C). In the side-on bridged structure, there is a Cu LUMO with significant peroxide π_o^* character because of the strong donor interaction of the peroxide with the Cu. In the bis-μ-oxo structure, the Cu-based LUMO now has significant σ^* character because of the strong oxide σ-donor interaction.

From model studies, both the π^* LUMO of the side-on peroxide and the σ^* LUMO of the bis-μ-oxo structures are capable of electrophilic reactions with aromatic substrates.

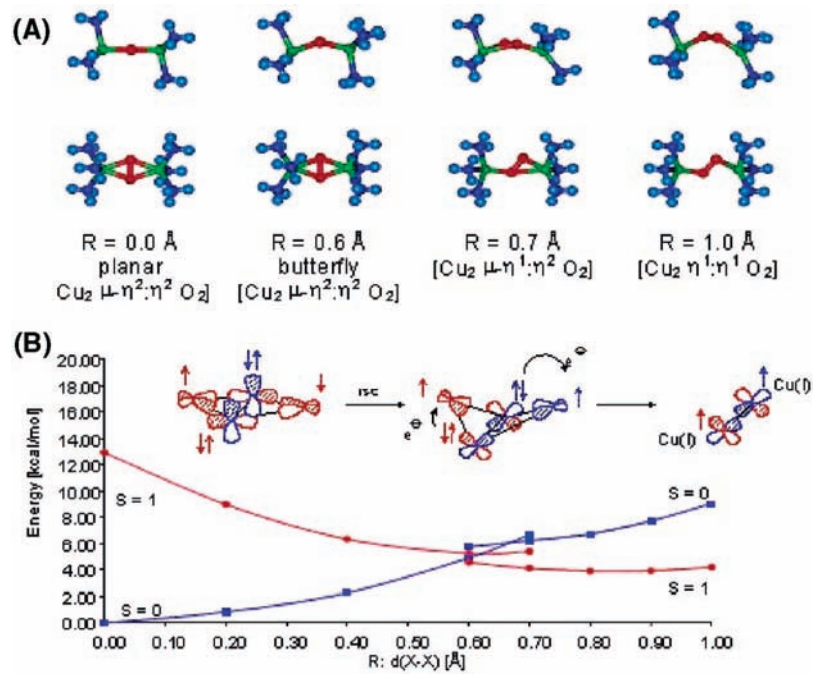

FIGURE 4. (A) Reaction coordinate of O_2 binding by Hc. View along the O–O (top) and perpendicular to the initial Cu_2O_2 plane (bottom). (B) Potential-energy surfaces for the interconversion of oxy-Hc and deoxy-Hc in triplet and singlet states. *R*:*d*(X–X) is the distance between the center of the O–O and Cu–Cu vectors. *R*:*d*(X–X) < ~0.6 and > ~0.6 represents symmetric and nonsymmetric O_2 coordination, respectively.

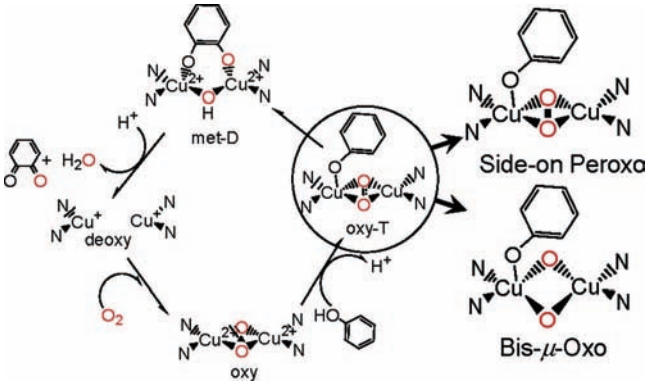

FIGURE 5. Molecular mechanism of the Ty catalysis. The two possible structures of substrate-bound oxy-T are expanded.

From Figure 7A, in the Karlin bidentate chelate ligand system,[11] an O_2 intermediate is trapped at a low temperature with an electron-withdrawing nitro substituent on the bridging ring. From rR data (Figure 7B), this species shows a ~750 cm^{-1} vibration characteristic of the side-on peroxo-bridged species, with no indication of a 600 cm^{-1} feature characteristic of the bis-μ-oxo species (upper limit of <0.1%).[12] As shown in parts B and C of Figure 7, the ~750 cm^{-1} feature decreases as the 1320 cm^{-1} feature, characteristic of the C–O stretch of the hydroxylated phenolate product, increases.

From Figure 8, the Stack diamine-ligated complex binds O_2 as the side-on peroxo-bridged species.[13] The addition of exogenous phenolate leads to the loss of the ~750 cm^{-1} ν_{O-O} vibration and appearance of the 600 cm^{-1} feature, characteristic of the bis-μ-oxo species. Thus, coordination of the phenolate to the Cu likely through a trigonal bipyramidal rearrangement into the equatorial

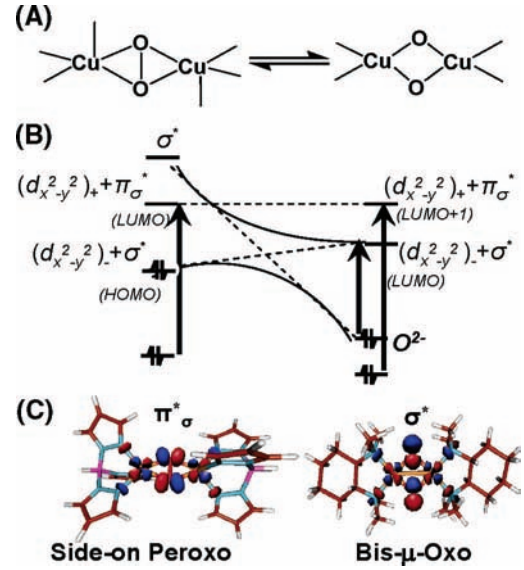

FIGURE 6. (A) Side-on peroxo (left) and bis-μ-oxo (right) correlation, (B) electronic structure correlation, and (C) FMOs (ie., LUMOs).

plane converts the side-on peroxide to the bis-μ-oxo species. This goes on to hydroxylate the phenolate to a mixture of catecholate and quinone products. Thus, both the side-on peroxo (through a π^* electrophilic mechanism) and the bis-μ-oxo (through a σ^* electrophilic mechanism) binuclear Cu sites can hydroxylate aromatic substrates.

3. Noncoupled Binuclear Cu Enzymes

PHM and DβM, involved in peptidic hormone production and the control of neurotransmitters, both catalyze substrate C–H bond hydroxylation by H-atom abstraction.[14]

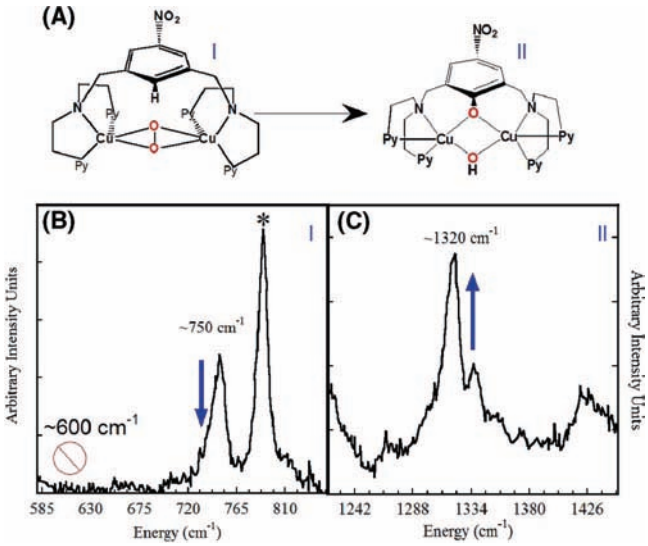

FIGURE 7. (A) Conversion of the side-on peroxide intermediate $[Cu_2(NO_2\text{–}XYL)(O_2)]^{2+}$ to $[Cu^{II}_2(NO_2\text{–}XYL\text{–}O^-)(OH)]^{2+}$. (B and C) Change in rR with time. The loss of the side-on peroxo stretch correlates with an increase of the C–O stretch.

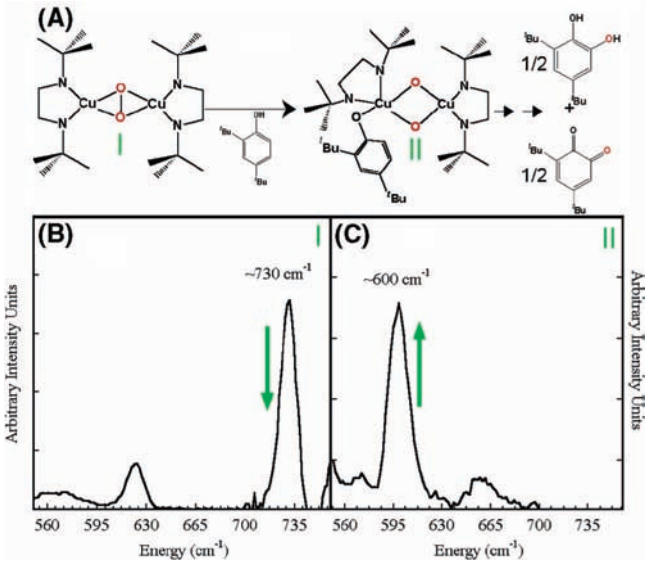

FIGURE 8. (A) Reaction of Side-on peroxo $\{[(DBED)Cu]_2O_2\}^{2+}$. (B and C) Change in rR with $(^tBu)_2Ph(O)^-$ coordination.

The active sites in these enzymes are noncoupled, in that they have two Cu^{II}'s, which each show spectroscopic features indicative of an isolated Cu^{II} $S = {}^1/_2$ center. This is consistent with the crystallography on PHM, which shows that the two Cu^{II}'s are 11 Å apart with no bridging ligation (only H_2O's in the interdomain cavity between the Cu's).[15] Reasonable descriptions of the geometric and electronic structure of each Cu^{II} center have been obtained through a combination of crystallography, extended X-ray absorption fine structure (EXAFS), magnetic circular dichroism (MCD) spectroscopy, and density functional theory (DFT) calculations.[16,17] As shown in Figure 9, Cu_M is the catalytic center, which has an axial Met, two equatorial His, and two equatorial H_2O/OH^- sites for O_2 reactivity. Cu_H has three His and a water ligand in a D_{2d}-distorted tetragonal geometry and supplies the extra e^-

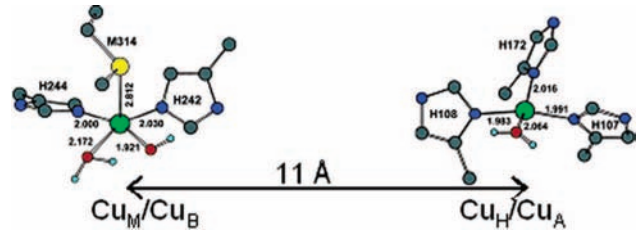

FIGURE 9. Geometry-optimized structures of the resting oxidized Cu_M and Cu_H sites in PHM.

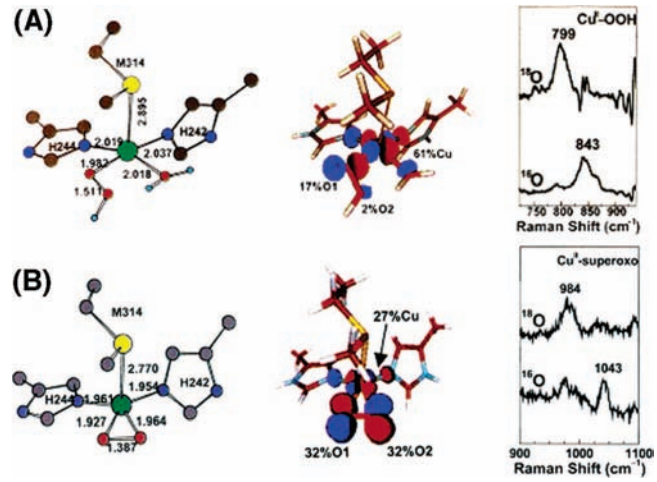

FIGURE 10. Electronic structure of the (A) Cu_M^{II}–OOH and (B) Cu_M^{II}–superoxo species. Geometry-optimized structure (left), acceptor FMO (LUMO) (middle), rR spectra in the ν_{O-O} region (right).

required for catalysis to Cu_M over a distance of 11 Å. There has been much discussion as to how this electron transfer (ET) might take place.[18]

Thus, the reaction of the noncoupled binuclear Cu enzymes requires O_2 activation by a single Cu center, which, until recently, was thought to involve a Cu_M^{II}–OOH species.[14] However, from spectroscopic and electronic structure studies on a Cu^{II}–hydroperoxide model complex, this species is not activated for H-atom abstraction.[19] From Figure 10A, the FMO only has 2% character on the distal oxygen for electrophilic attack, and from rR studies on the model, the ν_{O-O} is 843 cm^{-1} reflecting a strong O–O bond not activated for cleavage. This led us to studies of the alternative possibility of a $1e^-$ reduction of O_2 to generate a bound superoxo–Cu_M^{II} intermediate. From the rR data in Figure 10B, the ν_{O-O} of a η^2 O_2Cu model complex is 1043 cm^{-1}, which is characteristic of a Cu^{II}–O_2^- species; from its FMO, which has >60% O character, this species is strongly activated for electrophilic attack on H–C bonds.[20]

These predictions from model studies were strongly supported by electronic structure calculations of this reaction coordinate.[21] H-atom abstraction by the $2e^-$-reduced Cu_M^{II}–hydroperoxo species (blue curve in Figure 11) is endergonic and, in particular, has an activation barrier of 37 kcal/mol. Alternatively, H-atom abstraction by the $1e^-$-reduced Cu–superoxo species (red curve in Figure 11) is thermoneutral and has an activation barrier of only 14 kcal/mol, which is consistent with the FMO

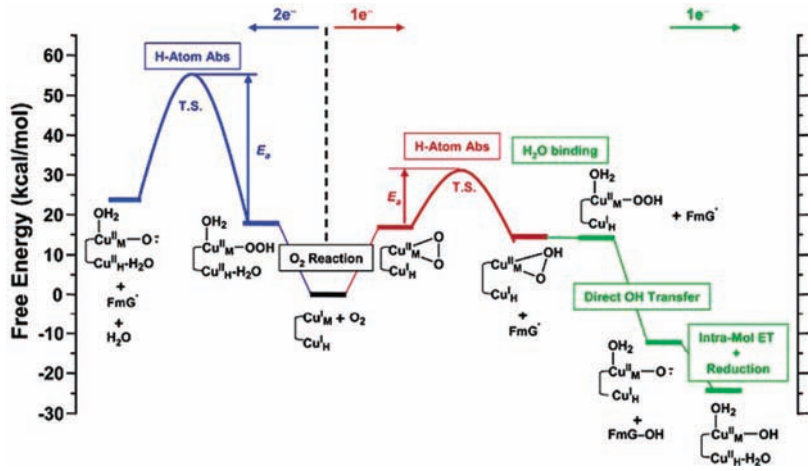

FIGURE 11. Summary of the $2e^-$ (blue) and $1e^-$ (red and green) reaction coordinates for the noncoupled binuclear Cu enzymes.

predictions. This would generate a Cu_M^{II}–OOH and substrate radical species, which would readily react via direct OH transfer from the hydroperoxide to generate the hydroxylated product and a Cu_M^{II}–$O^{\bullet -}$ (i.e., cupric–oxyl) species. This high-energy species would drive a proton-coupled ET from Cu_H to complete the reaction cycle.

A comparison of the reaction coordinates for the coupled binuclear Cu enzymes (Figure 5) and noncoupled binuclear Cu enzymes (Figure 11) shows an extremely important role of the differences in the AF exchange coupling (J) in the reaction mechanism. Rapid ET requires a large electronic coupling between the donor and acceptor (H_{DA}), which in turn is related to $J \propto (H_{DA})^2$.[21] Thus, large AF coupling leads to rapid ET. This is the case for the coupled binuclear Cu enzymes, where the large value of J between the Cu's via the bridging ligand leads to the $2e^-$ reduction of O_2 to form a Cu_2O_2 species capable of electrophilic aromatic attack. Alternatively, in these noncoupled binuclear Cu enzymes, J is very small because Cu_M and Cu_H are separated by an 11 Å solvent-filled cleft. The reduction of O_2 appears to proceed at one Cu via a $1e^-$-reduced Cu_M^{II}–O_2^- species, which is capable of H-atom abstraction. Such a Cu_MO_2 species has been observed in the crystal structure of PHM[22] and defined by rR in a model complex.[23] At a later stage of the reaction, a high-energy species is produced (the Cu_M^{II}–oxyl), which provides the large driving force required for ET from Cu_H with its low J (therefore, H_{DA}) with Cu_M.

4. Trinuclear Cu Cluster in the Multicopper Oxidases (MCOs)

The MCOs couple four $1e^-$ oxidations of substrates to the $4e^-/4H^+$ reduction of O_2 to H_2O.[1] These can be divided into two classes: one, as represented by laccase, uses organic substrates, which weakly to strongly interact with the protein near the type 1 (T1) Cu (*vide infra*), and the second, represented by Fet3p, has specific metal ion substrate-binding sites near the T1, which tune the metal ion potential and provide ET pathways to the T1.[24] The minimum structure of a MCO active site is shown in Figure 12A.

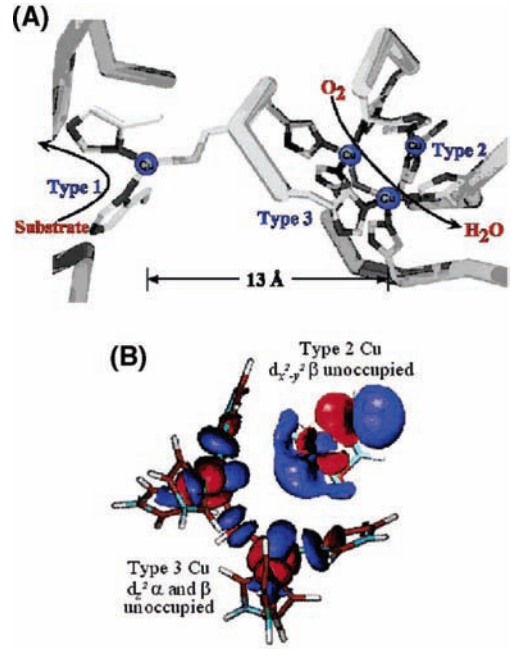

FIGURE 12. (A) Active site of the MCOs (AO is shown here). (B) Electronic structure of the trinuclear Cu cluster (TNC).

The T1 is a blue copper center capable of rapid ET through a Cys–His pathway, over 13 Å, to the trinuclear Cu cluster (TNC), where O_2 is reduced to H_2O. The TNC is comprised of a type 3 (T3) copper pair, where each Cu has three His ligands and the pair is strongly antiferromagnetically coupled (i.e., with a singlet ground state) through an OH^- bridge, and a type 2 (T2) center within 3.5 Å of the T3 Cu's, having two His and an OH^- ligand external to the cluster.[25] The T2 Cu is not bridged to the T3 Cu's and shows a normal Cu^{II} $S = {}^1/_2$ electron paramagnetic resonance (EPR) signal.

The electronic structure of the resting trinuclear Cu^{II} cluster is given in Figure 12B. This shows that all three Cu's have open coordination positions oriented inside the cluster. The coordination unsaturation of this highly positively charged cluster results from charged carboxylate residues within 8 Å of the cluster, which destabilize H_2O/OH^-/O^{2-} binding in the center of the cluster and thus tune its redox properties for O_2 reduction.[26]

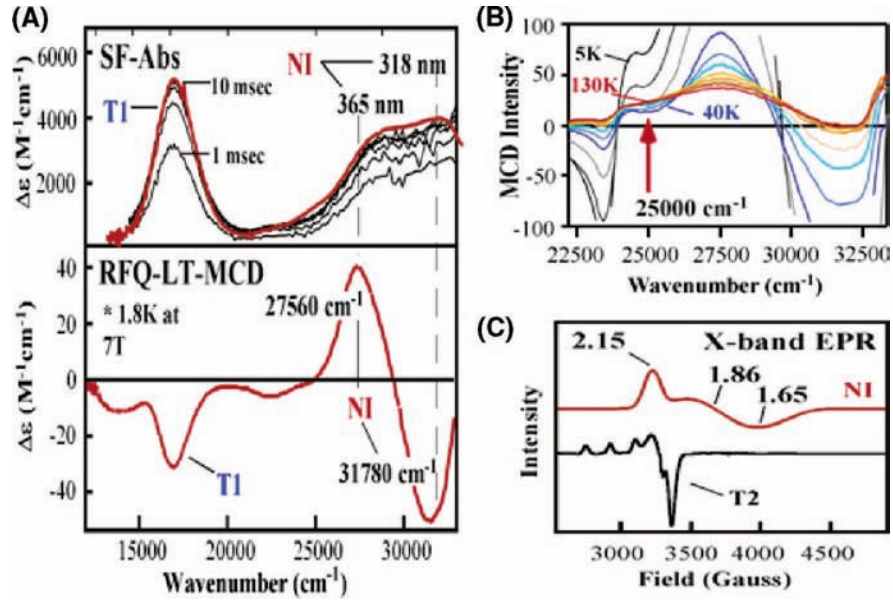

FIGURE 13. (A) Stopped-flow absorption showing the formation of NI, (B) rapid-freeze quench (RFQ)-LT-MCD spectrum of NI, (C) variable-temperature (VT-MCD) of NI, and (D) low-temperature X-band EPR spectrum of NI compared to resting T2.

O_2 intermediates were trapped to define the mechanism of O_2 reduction to H_2O by the MCOs. Initially, we studied a T1-depleted (T1D) derivative in laccase, where the T1 Cu was replaced by a redox-inactive Hg^{2+}.[27] Reduction of the TNC and reaction with O_2 led to the first intermediate. From a combination of isotope ratio mass spectrometry, circular dichroism (CD), and low-temperature (LT) MCD (which only probes paramagnetic centers), we determined that this was a peroxy intermediate with two coppers oxidized and AF-coupled and one copper reduced.[27] The AF coupling required a bridging ligand, and this was observed in EXAFS data on peroxy T1D, which showed two Cu's tightly bridged at 3.4 Å. Because one Cu was reduced in this intermediate, we could not directly study its interaction with the peroxide. Therefore, we prepared the peroxide adduct (PA) of the oxidized TNC in T1D.[28] PA showed the same Fourier transform (FT)-EXAFS feature at 3.4 Å, indicating a similar peroxide-binding mode, but now all Cu's are oxidized. Upon binding peroxide to the oxidized TNC, all of the ligand field features of the T2 and T3 Cu^{II}'s are perturbed, indicating an all bridged structure for the peroxide intermediate. This is consistent with the recent crystal structure of the peroxide adduct of oxidized CotA[29] and the quantum mechanics/molecular mechanics (QM/MM) energy-minimized structure of the peroxide intermediate.[30]

The reaction of the fully reduced native enzyme (i.e., $4Cu^{I}$) with O_2 generates the native intermediate (NI). As shown in Figure 13A, NI exhibits absorption features at 365 and 318 nm as well as an absorption band at 600 nm, associated with an oxidized T1 Cu.[31] Therefore, NI is at least one more electron-reduced relative to the peroxide intermediate. Associated with this, NI exhibits an unusual EPR signal (Figure 13C), with very unusual *g* values below 2.0. It is different from that of an oxidized T2 Cu^{II} and

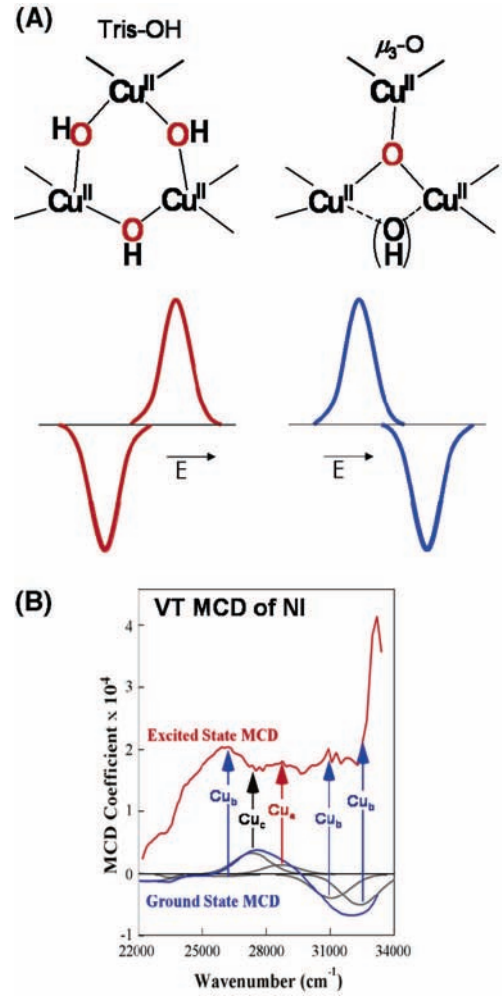

FIGURE 14. (A) Predicted and observed MCD signs for the two possible structures of NI and (B) ground- and excited-state MCD spectra of NI, where bands are grouped together according to their different temperature dependencies.

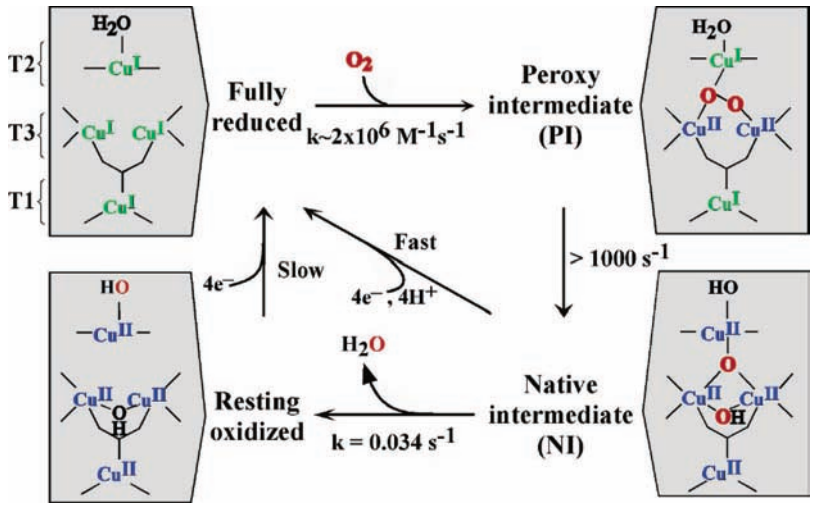

FIGURE 15. Mechanism of O_2 reduction to H_2O by the MCO's.

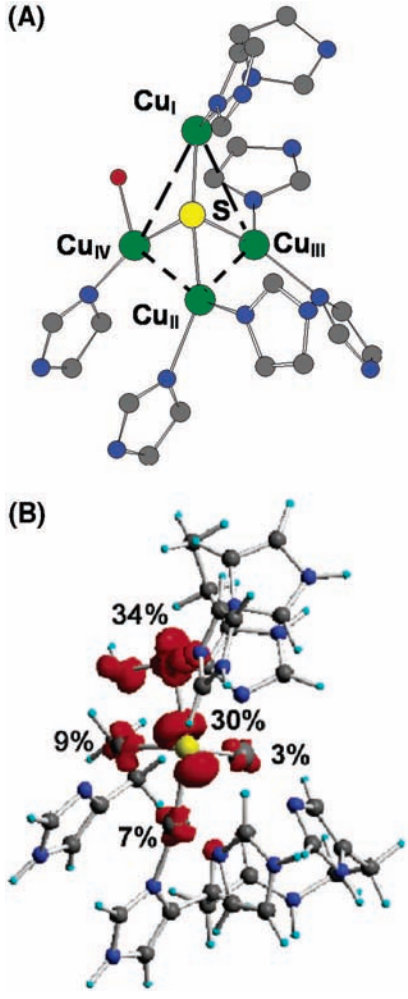

FIGURE 16. (A) Crystal structure (PnN_2OR). (B) Geometry-optimized electronic structure.

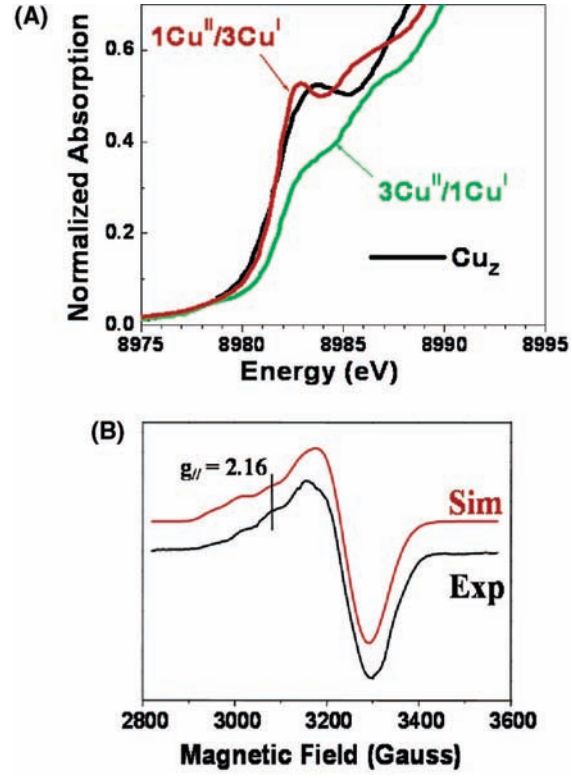

FIGURE 17. (A) Cu K-edge XAS spectrum of Cu_Z (black line) simulated with 1Cu^{II}/3Cu^{I} (red line) and 3Cu^{II}/1Cu^{I} (green line). (B) EPR spectrum of Cu_Z from PnN_2OR.

broadens when generated with $^{17}O_2$.[32] Thus, it had been assigned as an OH$^{\cdot}$ bound to a reduced T2 Cu. The most direct spectroscopic probe of reduced Cu is K-edge X-ray absorption spectroscopy (XAS) because Cu^{I} exhibits a characteristic feature at 8984 eV, not present in Cu^{II} complexes. It is also not present in NI.[31] Therefore, NI is a fully oxidized TNC but with an EPR signal very different from that of the fully oxidized TNC of the resting enzyme (Figure 13C), and dioxygen has been fully reduced to the H_2O level.

NI also has a characteristic derivative-shaped MCD signal associated with the 365/318 nm absorption bands known as a pseudo-A term (Figure 13A).[31] This has proven to be a direct probe of the geometric and electronic structure of NI. The field dependence of the MCD signal at low temperature gave a saturation magnetization curve, which fit to the Brillouin function for a $S = {}^1/_2$ ground state, associated with the unusual g values. The temper-

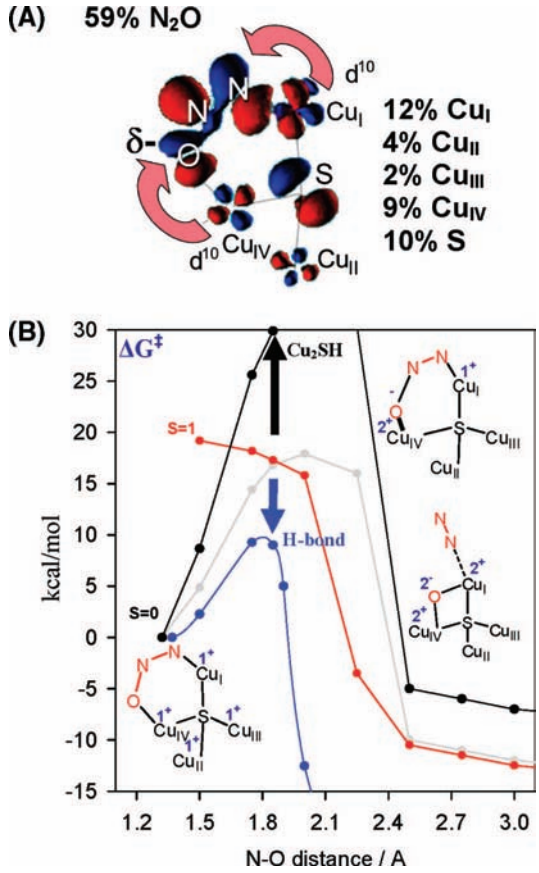

FIGURE 18. (A) Back-bonding interaction from fully reduced Cu_Z to N_2O. (B) N–O bond cleavage barrier of Cu_Z (red and gray lines), Cu_2SH (black line), and hydrogen-bond assisted (blue line).

ature dependence of the MCD signal at a fixed high magnetic field shows a very interesting behavior in Figure 13B. Normally, the MCD intensity of a paramagnetic $S = {}^1/_2$ center decreases as $1/T$. However, the MCD intensity in Figure 13B first decreases and then increases with increasing temperature, indicating the Boltzmann population of an excited state at 150 cm^{-1}, with a MCD signal different from that of the $S = {}^1/_2$ ground state of NI.

NI has an FT-EXAFS feature, indicating a bridged Cu–Cu distance of 3.3 Å, which would correspond to a pair of Cu^{II}'s of the trinuclear cluster site having a singlet/triplet splitting of ~520 cm^{-1}. Because we are dealing with a trinuclear Cu^{II} site, the singlet ground state of the pair couples with the third Cu^{II} to give a $S_{tot} = {}^1/_2$ ground state; the $S = 1$ excited state couples with the $S = {}^1/_2$ to form $S_{tot} = {}^1/_2$ and ${}^3/_2$ excited states. With a single bridge, this would produce a T2 EPR signal with g values above 2.0 and an excited state at 520 cm^{-1}. NI has a ground-state EPR signal with g values below 2.0 and an excited state at 150 cm^{-1}. Thus, we allow for additional AF exchange interactions (i.e., bridging ligands) between additional pairs of Cu^{II}'s of the TNC of NI. Allowing for a second bridge splits the excited $S_{tot} = {}^3/_2$ and ${}^1/_2$ states but does not bring the $S_{tot} = {}^1/_2$ first excited state below 440 cm^{-1} (~1.7J) and does not result in ground-state g values below 2.0. The addition of a third bridge now causes the $S = {}^1/_2$ excited state to greatly decrease in energy (this is a result of "spin frustration" because all three $S = {}^1/_2$ cannot be AF-coupled in a triangle) and the ground-state g values to decrease below 2.0 (because of antisymmetric exchange in the all-bridged trimer).[33] Thus, the experimental data on the ground and excited states of NI require all three Cu^{II}'s to be strongly exchange-coupled through bridging ligands.

There were two possible structures for NI where all Cu's are oxidized and bridged by the product of full O_2 reduction: a μ_3-oxo-bridged structure or a tris OH^--bridged structure, in which the third OH^- would derive from H_2O (top in Figure 14A). Model complexes exist with both structures, and both exhibit MCD pseudo-A terms (of opposite sign) associated with the hydroxo or oxo to Cu^{II} CT transitions of the trinuclear Cu^{II} cluster (bottom in Figure 14A).[34] The mechanism for pseudo-A terms requires two perpendicular CT transitions being spin-orbit-coupled in a third direction at one center. For the tris OH^- system, this would involve CT transitions from two OH^- ligands to one Cu^{II} center, which provides the spin-orbit coupling. For the μ_3-oxo structure, this involves oxo CT transitions to two Cu^{II} centers, which are spin-orbit-coupled by the oxo bridge. From the temperature-dependent MCD spectrum of NI shown in Figure 14B, the CT transitions forming the pseudo-A term involve different Cu centers, which is only consistent with a μ_3-oxo, all-bridged structure for NI.

The above spectroscopic studies of O_2 intermediates in the MCOs have led to the molecular mechanism of O_2 reduction to H_2O in Figure 15. The reduction of O_2 by the fully reduced MCO involves two $2e^-$ steps. From our kinetic studies, the first is rate-determining and the second is fast; therefore, it is effectively a $4e^-$ process.[1] The second step involves the $2e^-$ reductive cleavage of the O–O bond. It has a large driving force because of the $2e^-$ reduction potential of peroxide, and from mutagenesis studies, it is proton-assisted with a Glu near the T3, providing the proton for O–O bond cleavage. The NI is a fully oxidized form of the enzyme but is different from the resting form because it has an internal μ_3-oxo bridge. These interconvert, and the rate of decay of NI to the resting state is very slow because of the reorganization of the μ_3-oxo bridge (from O_2) to the external position on the T2 Cu^{II}. This decay of NI is too slow to be in the catalytic cycle, whereas the reduction of NI is fast (>1000 s^{-1}),[35] and this is the catalytically relevant fully oxidized form of the MCOs. ET from the T1 to the TNC is fast because the μ_3-oxo bridge provides an effective superexchange pathway to the T2 Cu.

5. μ_4-Sulfide Bridged Tetranuclear Cu_Z Cluster in Nitrous Oxide Reductase

The tetranuclear Cu_Z cluster catalyzes the $2e^-/2H^+$ cleavage of the N–O bond in N_2O.[36] From the crystal structure, electrons enter at the mixed valent binuclear Cu_A center of one subunit and are transferred over a 10 Å superexchange pathway to the Cu_Z cluster of a second subunit where N_2O reduction occurs at the Cu_I/Cu_{IV} edge (Figure

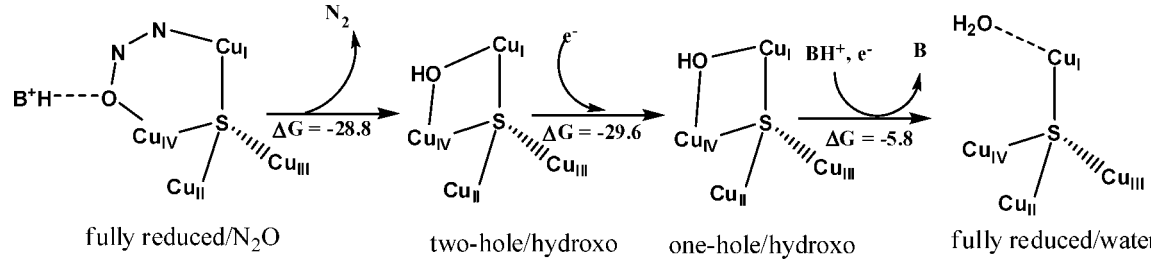

FIGURE 19. N_2OR reaction mechanism.

16A). The μ_4-SCu_4 cluster is held in the protein by seven His ligands, two on Cu_I–Cu_{III} and one on Cu_{IV}. In the resting crystal structures, there are one or two H_2O-derived ligands at the Cu_I/Cu_{IV} edge.[36,37]

The initial goal of spectroscopy was to determine the electronic structure of the crystallographically defined resting Cu_Z cluster.[38] The Cu_Z cluster has a sulfide to Cu CT transition at 640 nm, which shows a pseudo-A term MCD spectrum. The temperature dependence of the MCD shows that the ground state has $S_{tot} = {}^1/_2$, which can either reflect a site with $1Cu^{II}/3Cu^{I}$ or $3Cu^{II}/1Cu^{I}$. These possibilities could be distinguished with XAS at the Cu K-edge, where, from Figure 17A, the Cu_Z feature at 8984 eV shows that three Cu's are reduced in the resting Cu_Z cluster.[39] This leaves one hole on the cluster, and its distribution could be determined by a combination of X- and Q-band EPR and S K-edge XAS. Figure 17B shows that the $g_{||}$ value from Q band lies on a Cu hyperfine line in the X band, requiring e^- delocalization over at least two Cu's. These experimental results are supported by geometry-optimized DFT calculations (Figure 16B), which show dominant Cu_I character but significant delocalization of the hole over the cluster depending upon the nature of the edge ligand.[39]

The edge ligand could be detected by rR spectroscopy, which also elucidated the requirement of a proton for high activity of N_2OR. A structural model consistent with the results involves an OH^- edge ligand, whose orientation is affected by hydrogen bonding to a protonated Lys at the Cu_I/Cu_{IV} edge. This protonated Lys appears to play a significant role in assisting catalysis.

We next focus on the redox state of Cu_Z required for catalysis. Reduction of the Cu_Z EPR signal of the one-hole form directly correlates with the activity. Thus, the fully reduced ($4Cu^I$) form of the Cu_Z reacts with N_2O in catalysis.[39] Geometry optimization of N_2O at the Cu_I/Cu_{IV} edge shows that it binds as a μ-1,3 bridge, bent with an angle of 139°. From Figure 18A, this bending greatly lowers the energy of the π^* LUMO of N_2O, which leads to extensive back bonding from fully reduced Cu_Z into the N_2O, activating the cleavage of the N–O bond.[39]

Figure 18B evaluates the potential energy surface for N–O cleavage on the Cu_Z cluster. The barrier is reduced from 61 kcal/mol in the gas phase to 18 kcal/mol on Cu_Z. This is because the bent N_2O reactant is destabilized and, in particular, the extensive back bonding lowers the TS energy through stabilization of the Cu^{II}_{IV}–O^- bond. Allowing for a protonated ligand to hydrogen bond to this oxo further lowers the TS to ~10 kcal/mol. Finally, because the two e^- transferred are donated from Cu_I and Cu_{IV}, it is interesting to evaluate the role of the additional Cu's in the cluster. Eliminating Cu_{II} and Cu_{III} (and saturating the sulfide by protonation) eliminates much of the back bonding into N_2O and increases the barrier for N–O cleavage to 37 kcal/mol.[40]

The above considerations lead to the molecular mechanism for the $2e^-/2H^+$ cleavage of N_2O shown in Figure 19. Hydrogen bonding from the protonated Lys lowers the barrier for N–O cleavage, which leads to the two-hole hydroxyl-bridged species. This is rapidly reduced by Cu_A to the one-hole species, where protonation of the Lys again raises the potential and provides a proton to complete the reaction cycle.[40]

6. Concluding Comments

Spectroscopic/electronic structure studies on the intermediates and model complexes of copper proteins have provided fundamental insights into their reactivities. Among major issues that remain are the structural differences over the coupled binuclear copper proteins that lead to their different reactivities in Figure 1, whether the side-on structure of oxy-Ty directly reacts with substrates or converts to the bis-μ-oxo structure along the reaction coordinate of phenolate binding and hydroxylation in Figure 5, the reactivity of the Cu^{II} O_2^- species in H-atom abstraction and its relevance to the PHM mechanism in Figure 11, the fundamental differences of the trinuclear copper cluster in the multicopper oxidases relative to the coupled binuclear copper protein sites in dioxygen reactivity and the factors involved in the proton-assisted reductive cleavage of the O–O bond, and trapping and defining the key intermediates in the reaction mechanism of N_2OR in Figure 19. The field of copper bioinorganic chemistry has come a long way, but there is still much to understand.

We thank past students and collaborators who have greatly contributed to this work and the NIH (DK31450) for funding.

References

(1) Solomon, E. I.; Sundaram, U. M.; Machonkin, T. E. Multicopper oxidases and oxygenases. *Chem. Rev.* **1996**, *96*, 2563–2605.
(2) Pate, J. E.; Cruse, R. W.; Karlin, K. D.; Solomon, E. I. Vibrational, electronic, and resonance Raman spectral studies of $(Cu_2(XYL–O–)\text{-}O_2)^+$, a copper(II) peroxide model complex of oxyhemocyanin. *J. Am. Chem. Soc.* **1987**, *109*, 2624–2630.

(3) Baldwin, M. J.; Ross, P. K.; Pate, J. E.; Tyeklár, Z.; Karlin, K. D.; Solomon, E. I. Spectroscopic and theoretical studies of an end-on peroxide-bridged coupled binuclear copper(II) model complex of relevance to the active sites in hemocyanin and tyrosinase. *J. Am. Chem. Soc.* **1991**, *113*, 8671–8679.

(4) Baldwin, M. J.; Root, D. E.; Pate, J. E.; Fujisawa, K.; Kitajima, N.; Solomon, E. I. Spectroscopic studies of side-on peroxide-bridged binuclear copper(II) model complexes of relevance to oxyhemocyanin and oxytyrosinase. *J. Am. Chem. Soc.* **1992**, *114*, 10421–10431.

(5) Metz, M.; Solomon, E. I. Dioxygen binding to deoxyhemocyanin: Electron structure and mechanism of the spin forbidden two-electron reduction of O_2. *J. Am. Chem. Soc.* **2001**, *123*, 4938–4950.

(6) Solomon, E. I.; Baldwin, M. J.; Lowery, M. D. Electronic structures of active sites in copper proteins: Contributions to reactivity. *Chem. Rev.* **1992**, *92*, 521–542.

(7) Solomon, E. I.; Chen, P.; Metz, M.; Lee, S. K.; Palmer, A. E. Oxygen binding, activation, and reduction to water by copper proteins. *Angew. Chem., Int. Ed.* **2001**, *40*, 4570–4590.

(8) Halfen, J. A.; Mahapatra, S.; Wilkinson, E. C.; Kaderli, S.; Young, V. G.; Que, L.; Zuberbuhler, A. D.; Tolman, W. B. Reversible cleavage and formation of the dioxygen O–O bond within a dicopper complex. *Science* **1996**, *271*, 1397–1400.

(9) DuBois, J. L.; Mukherjee, P.; Collier, A. M.; Mayer, J. M.; Solomon, E. I.; Hedman, B.; Stack, T. D. P.; Hodgson, K. O. Cu K-edge XAS study of the $[Cu_2(\mu\text{-}O)_2]$ core: Direct experimental evidence for the presence of Cu(III). *J. Am. Chem. Soc.* **1997**, *119*, 8578–8579.

(10) Henson, M. J.; Mukherjee, P.; Root, D. E.; Stack, T. D. P.; Solomon, E. I. Spectroscopic and electronic structural studies of the $Cu(III)_2$ bis-μ-oxo core and its relation to the side-on peroxo-bridged dimer. *J. Am. Chem. Soc.* **1999**, *121*, 10332–10345.

(11) Karlin, K. D.; Nasir, M. S.; Cohen, B. I.; Cruse, R. W.; Kaderli, S.; Zuberbuehler, A. D. Reversible dioxygen binding and aromatic hydroxylation in O_2 reactions with substituted xylyl dinuclear copper(I) complexes: Syntheses and low-temperature kinetic/thermodynamic and spectroscopic investigations of a copper monooxygenase model system. *J. Am. Chem. Soc.* **1994**, *116*, 1324–1336.

(12) Pidcock, E.; Obias, H. V.; Zhang, C. X.; Karlin, K. D.; Solomon, E. I. Investigation of the reactive oxygen intermediate in an arene hydroxylation reaction performed by xylyl-bridged binuclear copper complexes. *J. Am. Chem. Soc.* **1998**, *120*, 7841–7847.

(13) Mirica, L. M.; Vance, M.; Rudd, D. J.; Hedman, B.; Hodgson, K. O.; Solomon, E. I.; Stack, T. D. P. Tyrosinase reactivity in a model complex: An alternative hydroxylation mechanism. *Science* **2005**, *308*, 1890–1892.

(14) Klinman, J. P. Mechanisms whereby mononuclear copper proteins functionalize organic substrates. *Chem. Rev.* **1996**, *96*, 2541–2561.

(15) Prigge, S. T.; Kolhekar, A. S.; Eipper, B. A.; Mains, R. E.; Amzel, L. M. Amidation of bioactive peptides: The structure of peptidylglycine α-hydroxylating monooxygenase. *Science* **1997**, *278*, 1300–1305.

(16) Blackburn, N. J.; Rhames, F. C.; Ralle, M.; Jaron, S. Major changes in copper coordination accompany reduction of peptidylglycine monooxygenase: Implications for electron transfer and the catalytic mechanism. *J. Biol. Inorg. Chem.* **2000**, *5*, 341–353.

(17) Chen, P.; Bell, J.; Eipper, B. A.; Solomon, E. I. Oxygen activation by the noncoupled binuclear copper site in peptidylglycine α-hydroxylating monooxygenase. Spectroscopic definition of the resting sites and the putative $Cu_M(II)$–OOH intermediate. *Biochemistry* **2004**, *43*, 5735–5747.

(18) Francisco, W. A.; Wille, G.; Smith, A. J.; Merkler, D. J.; Klinman, J. P. Investigation of the pathway for inter-copper electron transfer in peptidylglycine α-amidating monooxygenase. *J. Am. Chem. Soc.* **2004**, *126*, 13168–13169.

(19) Chen, P.; Fujisawa, K.; Solomon, E. I. Spectroscopic and theoretical studies of mononuclear copper(II) alkyl- and hydroperoxo complexes: Electronic structure contributions to reactivity. *J. Am. Chem. Soc.* **2000**, *122*, 10177–10193.

(20) Chen, P.; Root, D. E.; Campochiaro, C.; Fujisawa, K.; Solomon, E. I. Spectroscopic and electronic structure studies of the diamagnetic side-on Cu^{II}–superoxo complex $Cu(O_2)[HB(3\text{-}R\text{-}5\text{-}^iPrpz)_3]$: Antiferromagnetic coupling versus covalent delocalization. *J. Am. Chem. Soc.* **2003**, *125*, 466–474.

(21) Chen, P.; Solomon, E. I. O_2 activation by binuclear Cu sites: Noncoupled versus exchange coupled reaction mechanisms. *Proc. Natl. Acad. Sci. U.S.A.* **2004**, *101*, 13105–13110.

(22) Prigge, S. T.; Eipper, B. A.; Mains, R. E.; Amzel, L. M. Dioxygen binds end-on to mononuclear copper in a precatalytic enzyme complex. *Science* **2004**, *304*, 864–867.

(23) Maiti, D.; Fry, H. C.; Woertink, J. S.; Vance, M. A.; Solomon, E. I.; Karlin, K. D. A 1:1 copper–dioxygen adduct is an end-on bound superoxo copper(II) complex which undergoes oxygenation reactions with phenols. *J. Am. Chem. Soc.* **2007**, *129*, 264–265.

(24) Quintanar, L.; Gebhard, M.; Wang, T. P.; Kosman, D. J.; Solomon, E. I. Ferrous binding to the multicopper oxidases *Saccharomyces cerevisiae* Fet3p and human ceruloplasmin: Contributions to ferroxidase activity. *J. Am. Chem. Soc.* **2004**, *126*, 6579–6589.

(25) Messerschmidt, A.; Ladenstein, R.; Huber, R.; Bolognesi, M.; Avigliano, L.; Petruzzelli, R.; Rossi, A.; Finazziagro, A. Refined crystal structure of ascorbate oxidase at 1.9 Å resolution. *J. Mol. Biol.* **1992**, *224*, 179–205.

(26) Quintanar, L.; Yoon, J.; Aznar, C. P.; Palmer, A. E.; Andersson, K. K.; Britt, R. D.; Solomon, E. I. Spectroscopic and electronic structure studies of the trinuclear Cu cluster active site of the multicopper oxidase laccase: Nature of its coordination unsaturation. *J. Am. Chem. Soc.* **2005**, *127*, 13832–13845.

(27) Shin, W.; Sundaram, U. M.; Cole, J. L.; Zhang, H. H.; Hedman, B.; Hodgson, K. O.; Solomon, E. I. Chemical and spectroscopic definition of the peroxide-level intermediate in the multicopper oxidases: Relevance to the catalytic mechanism of dioxygen reduction to water. *J. Am. Chem. Soc.* **1996**, *118*, 3202–3215.

(28) Sundaram, U. M.; Zhang, H. H.; Hedman, B.; Hodgson, K. O.; Solomon, E. I. Spectroscopic investigation of peroxide binding to the trinuclear copper cluster site in laccase: Correlation with the peroxy-level intermediate and relevance to catalysis. *J. Am. Chem. Soc.* **1997**, *119*, 12525–12540.

(29) Bento, I.; Martins, L. O.; Lopes, G. G.; Carrondo, M. A.; Lindley, P. F. Dioxygen reduction by multi-copper oxidases; a structural perspective. *J. Chem. Soc., Dalton Trans.* **2005**, 3507–3513.

(30) Rulisek, L.; Solomon, E. I.; Ryde, U. A combined quantum and molecular mechanical study of the O_2 reductive cleavage in the catalytic cycle of multicopper oxidases. *Inorg. Chem.* **2005**, *44*, 5612–5628.

(31) Lee, S. K.; George, S. D.; Antholine, W. E.; Hedman, B.; Hodgson, K. O.; Solomon, E. I. Nature of the intermediate formed in the reduction of O_2 to H_2O at the trinuclear copper cluster active site in native laccase. *J. Am. Chem. Soc.* **2002**, *124*, 6180–6193.

(32) Aasa, R.; Branden, R.; Deinum, J.; Malmstrom, B. G.; Reinhammar, B.; Vanngard, T. A ^{17}O-effect on EPR spectrum of intermediate in dioxygen–laccase reaction. *Biochem. Biophys. Res. Commun.* **1976**, *70*, 1204–1209.

(33) Yoon, J.; Mirica, L. M.; Stack, T. D. P.; Solomon, E. I. Spectroscopic demonstration of a large antisymmetric exchange contribution to the spin-frustrated ground state of a D_3 symmetric hydroxy-bridged trinuclear Cu(II) complex: Ground-to-excited state superexchange pathways. *J. Am. Chem. Soc.* **2004**, *126*, 12586–12595.

(34) Yoon, J.; Mirica, L. M.; Stack, T. D. P.; Solomon, E. I. Variable-temperature, variable-field magnetic circular dichroism studies of tris-hydroxy- and μ_3-oxo-bridged trinuclear Cu(II) complexes: Evaluation of proposed structures of the native intermediate of the multicopper oxidases. *J. Am. Chem. Soc.* **2005**, *127*, 13680–13693.

(35) Cole, J. L.; Ballou, D. P.; Solomon, E. I. Spectroscopic characterization of the peroxide intermediate in the reduction of dioxygen catalyzed by the multicopper oxidases. *J. Am. Chem. Soc.* **1991**, *113*, 8544–8546.

(36) Zumft, W. G.; Kroneck, P. M. H. Respiratory transformation of nitrous oxide (N_2O) to dinitrogen by bacteria and archaea. *Adv. Microb. Phys.* **2006**, *52*, 107–227.

(37) Brown, K.; Tegoni, M.; Prudencio, M.; Pereira, A. S.; Besson, S.; Moura, J. J.; Moura, I.; Cambillau, C. A novel type of catalytic copper cluster in nitrous oxide reductase. *Nat. Struct. Biol.* **2000**, *7*, 191–195.

(38) Rasmussen, T.; Berks, B. C.; Sanders-Loehr, J.; Dooley, D. M.; Zumft, W. G.; Thomson, A. J. The catalytic center in nitrous oxide reductase, Cu_Z, is a copper-sulfide cluster. *Biochemistry* **2000**, *39*, 12753–12756.

(39) Chen, P.; Gorelsky, S. I.; Ghosh, S.; Solomon, E. I. N_2O reduction by the μ_4-sulfide-bridged tetranuclear Cu_Z cluster active site. *Angew. Chem., Int. Ed.* **2004**, *43*, 4132–4140.

(40) Gorelsky, S. I.; Ghosh, S.; Solomon, E. I. Mechanism of N_2O reduction by the μ_4-S tetranuclear Cu_Z cluster of nitrous oxide reductase. *J. Am. Chem. Soc.* **2006**, *128*, 278–290.

AR600060T